DOI: 10.21062/mft.2022.078 http://www.journalmt.com

ATF Claddings after High-Temperature Steam Oxidation: WDS and Nanoindentation Studies to Characterize in-depth Material Changes

Jitka Klaisnerová (0000-0002-7314-7121)[1], Leoš Křivský (0000-0002-7640-1674)[1], Petra Gávelová (0000-0002-3789-3805)[1], Jakub Krejčí[2]
[1]Centrum výzkumu Řež s.r.o., Hlavní 130, 250 68 Husinec - Řež. Czech Republic. E-mail: jitka.klaisnerova@cvrez.cz, leos.krivsky@cvrez.cz, petra.gavelova@cvrez.cz.
[2] ÚJP PRAHA a.s., Nad Kamínkou 1345, 156 00 Zbraslav, Czech Republic. E-mail: jakub.krejci@cvrez.cz.

After the Fukushima accident in 2011 year, ATF nuclear fuel cladding concept was accelerated to achieve the reactor operation with the new accident tolerant structural materials. However, several designed solutions do not fulfil the accident tolerant concept but particularly increase the corrosion resistance of Zr-cladding tubes at normal operating conditions, so-called "Advanced Technology Fuel, EATF". Cr-coated zirconium claddings following the first concept, have been the widely tested and the first full Cr-coated fuel rods have been planned to operate in LWR reactor conditions around the 2022 year. Our contribution describes the Cr-coated Zr-%1Nb cladding tube microstructure after high-temperature steam oxidation at 1200°C by means of Scanning Electron Microscopy and nanoindentation methods. The article is focused on WDS line-profile studies of oxygen and chromium diffusion into the Zr-matrix. The increased Cr-diffusion with oxygen is evident causing a change in local mechanical properties which is well-described by measurements of nanohardness and Young's modulus. In addition, the developed methodology of the WDS & nanoindentation line-analyses was also optimized to apply in hot-cell conditions to measure the effect of neutron-irradiation on the different coatings and coating/matrix interface.

Keywords: Cladding tubes, ATF, WDS, EDS, high-temperature oxidation, nanoindentation.

1 Introduction

Due to a good balance between resistance to corrosion, neutron transparency and mechanical properties, zirconium-based alloys have been used since the 1960s for nuclear fuel claddings in Light Water Reactors (LWRs) [1]. Preserving the good mechanical properties and integrity of the fuel cladding is crucial not only for the reactor operation, but also for the following wet and dry storage and transportation of the spent fuel rods [2]. In addition, this role becomes more important during loss of coolant (LOCA) and severe accidents [3]. After Fukushima Daiichi accident in 2011 year, the development of alternative nuclear fuel materials to increase the safety in severe conditions was revived – focusing to replace or improve the currently used Zr-alloys, so-called Accident Tolerant Fuels, ATF (reducing heat and hydrogen production by high-temperature reaction with steam during loss of cooling) [3]. Improvement of current Zr-claddings is based on their deposition by Cr, CrN-thin coatings using different deposition methods, while the replacement of the verified Zr-alloys is discussed by refractory alloys as Ti, Ni-based alloys or alloy composition tuning with aluminium addition (intensively studied FeCrAl), F/M steels, ceramic materials (SiC_f, SiC), prospective materials (HEA/CCA/MAX phases), etc. On the fuel side, research on enhanced performance has focused on improved UO_2 (doped with oxides such as Cr_2O_3, Al_2O_3 or SiO_2, or with high-thermal-conductivity metallic or ceramic phases, to enhance the fission gas release process by increasing the grain size and optimize mechanical properties), higher density fuels (nitrides, carbides, silicides and metals), or micro-encapsulated fuels [4].

Focused on the improvement of currently used Zr-based alloys, the one ATF fuel cladding concept which has been fully used in nuclear reactor is the Enhanced ATF type (EATF) based on the Cr-coating deposited on the currently used Zr-claddings, while stoichometric CrN and multi-layer type of ATF as Cr + CrN-based are still in development [5]. Mostly in USA, ATF activities led to funding of collaborative research by fuel manufacturers Westinghouse, Framatome and GNF to give the first ATF rods into the USA nuclear power plants (NPPs) by 2022 year. There are a several benefits as well as disadvantage to use Cr-coated claddings in the current reactor generation [4]:

- EATF does not change the design and the manufacturing process of claddings, it means the minimum impact to the licensing process. (+),
- EATF type reduces the fuel corrosion at normal reactor operation and therefore icreases the fuel burnup. (+),
- LTA with several fuel rods is already irradiated in NPPs in Europe as well as USA. There is active research in the EATF – regular transport of the fuel rods from NPPs into hot-cell laboratories for qualification experiments which probably allows to realize the reactor operation with EATF in the close future. (+),
- Cr reacts with Zr-alloys at the temperature above 1305°C and then stops the protective properties of the Cr-coating. In this case, EATF will add only tens of minutes to efficient cooling recovery compared to the standard Zr-cladding tubes. (-).

The EATF type then brings the advantage particularly in normal reactor operation and slightly in severe accidents conditions, therefore the behavior of the Cr-coated should be well-described at LWR conditions [4].

After high-temperature oxidation (HTO), a typical Cr_2O_3 rhombohedral crystallographic structure with a particular crystallographic texture, the (001) crystallographic planes being mainly perpendicular to the coating surface [4]. A continuous chromium-zirconium thick layer at the Cr/prior-βZr interface. This layer is due to the inter-diffusion between the Zr substrate and the Cr coating occurring upon the incursion at high-temperature. Consistently with the Zr-Cr phase diagram, it was observed that this thin layer is constituted mainly of an intermetallic $Zr(Cr,Fe)_2$ C15 (face centered cubic, fcc) Laves phase [4].

Interaction between coating and substrate as chromium diffusion into the substrate and zirconium diffusion into coating along grain boundaries was described by several author teams [1], [6]. Our contribution is focused on the analysis of chromium, zirconium and niobium diffusion during high-temperature oxidation for 9 min at 1200 °C.

2 Materials and methods

2.1 Material and coatings

The tests presented in this paper were performed using the Zr-1%Nb cladding alloy. The tested tubular non-irradiated segments had an outer diameter of 9.1 mm and a length of 45 mm, and the thickness of the wall was about 0.6 mm. Tubular segments were sealed with Zr-1%Nb end-plugs, and welding was performed using the electron beam method.

The chromium coating was deposited on the outer surfaces of specimens by physical vapour deposition (magnetron sputtering) using the Hauzer Flexicoat 850 industrial system. Specimens were ultrasonically cleaned in: acetone, ethanol, and demineralized water. And in the end dried with a blower before coating deposition. The tubes were placed into a vacuum chamber on rotating holders where the tube surfaces were cleaned by ion etching in the argon plasma. This process removes the thin Zr-oxide and other impurities, thus improving the adhesion of the coating. The thickness of the coatings after the deposition was measured with an optical microscope and LUCIA G image analyzer and was found to be 10.6 ± 0.2 μm for the Cr layer.

2.2 High-temperature steam oxidation

Coated tubular segments were cleaned, degreased, and then weighted, and then exposed for variable time intervals to high-temperature steam at low pressure (0.1 MPa). The test was performed in a resistance furnace at a constant temperature. The oxidation was single-sided. An S-type thermocouple measured the temperature placed close to the specimen surface. At the end of the test, the sample was quenched in ice water.

2.3 Sample preparation for material characterization

For WDS analysis, EDS analysis and nanoindentation, the sample was metallographically ground and polished. Then, fine polishing was performed on MD-Dac, wetting agent DiaPro Dac 3 μm (diamond suspension for polishing), rotation speed 150 rpm, pressure 30 N/sample, for 05:00 min. Furthermore, fine polishing was performed on MD-Nap (cloth with acetate surface for polishing), wetting agent DiaPro Dac 1μm (diamond suspension for polishing), rotation speed 150 rpm, pressure 30 N/1 sample, for 05:00 min. The samples were purified with water in a Lavamin ultrasonic cleaner from Struers.

2.4 WDS and nanoindentation: line-profile analysis after HTO

BSE imaging and microchemical analysis using WDS line profiles were performed on a SEM Tescan MIRA3 GMU equipped with a Field Emission Gun (FEG) auto-emission cathode, fitted with Wave700 inclined WDS Spectrometer (Oxford Instruments), at the accelerating voltage of 15kV and beam current of 35nA. Standardization was performed using SPI standards of pure elements Fe, Cr, Zr, Nb and compound ZrO_2-Y for the analysis of oxygen.

WDS line profiles were acquired across the outer tube wall including coating into the substrate with the set distance of analytical points of 2 μm. The first point of the WDS profile was set to the resin, the last to the substrate. The first point included to the evaluation was selected according to chromium concentration (resin analytical points without chromium). A total of 3 WDS line profiles were acquired to the depth of 200 μm from the coating/substrate interface to the substrate. The WDS line profiles were 13 μm apart. A analysis area is shown in Figure 1.

Nanoindentation was performed with Hysitron Ti 950 nanoindenter with low force modulus head and Berkovich diamond tip along the WDS profiles. Each indentation profile consisted of 70 indents separated by 3 μm. Basic trapezoid load function was selected. This load function had 2 seconds loading segment to maximal force, 1 second hold segment at maximal force and 2 seconds unloading segment to zero force. Stage and tip drift was measured 60 and 45 seconds and were included in the hardness calculations. The maximum load 3 mN was selected to reach indents size about 1 μm wide. The beginning of indention profile was placed to resin to ensure that the indents at the beginning of the profile extend into the coating-matrix interface. Finally, the nanoindentation curves were evaluated by the Oliver-Phar method in Triboscan and Niget software. A analysis area is shown in Figure 1.

The sample was analyzed by EDS. An overview map (view field 220 um) and a detailed map of the oxide layer, coating and part of the substrate were created.

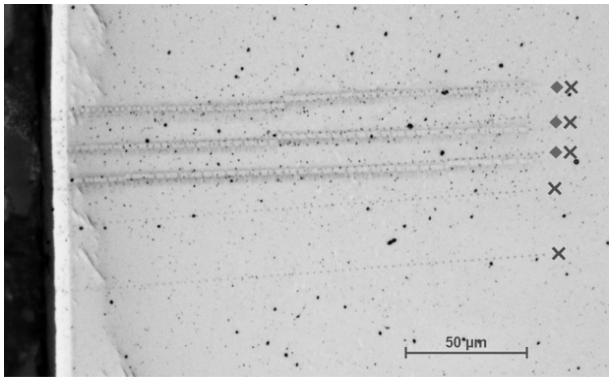

Fig. 1 *The area of interest: Rhombus – WDS analysis profile; cross – nanoindentation profile*

3 Results and discussion

The coating/substrate interface was chosen as the zero point of analysis, therefore the oxidation layer and coating are in negative values.

Data from WDS analysis and nanoindentation were averaged and presented in Graph 1-4.

The Cr content in the oxide layer (Graph 1) increases until the transition to the chromium layer, where it reaches the highest value of 98.44 % at a distance of -4 μm. At the coating/substrate boundary at a distance of 0 μm, the Cr content decreases to 3.06 %. From this point, the Cr concentration decreases up to about 190 μm where the concentration reaches 0 % (Graph 2). The weight percentage of Nb in the coating region increases at a distance of -2 μm (Graph 1). In the substrate, the Nb concentration is constant (Graph 2).

The results of nanoindentation hardness compared with chromium weight concentration are presented in Graph 3-4. The first indents (at a distance of 0 to 3 μm) extend into the chromium oxides. The highest hardness value was measured here, namely (11.68 ± 4.61) GPa (Graph 3). The high hardness is due to the presence of Cr_xO_y oxides (CrO_2, Cr_2O_3) produced by high-temperature oxidation in the steam [7]. WDS data of elements weight concentration is presented in Graph 1. The amount of oxygen decreased from 38 weight percent at -10 μm distance to 20.35 weight percent at -6 μm distance which means chromium oxides with higher proportion of oxygen on the surface of the sample. The presence of more different oxides results in high hardness and at the same time a higher standard deviation, where the lower cohesion of the oxide layer also plays a role [8].

The second indents (at a distance of -7 to -1 μm) extend into unoxidized chromium. Here, a significant decrease in hardness compared to the oxide layer was measured to a value of (4.15 ± 0.16) GPa. Values abouth 2 GPa were measured by nanoindentation of high-purity chromium by Christian Brandl and his team at room temperature. Their study of chromium of various purities also showed that with just a 0.2 % increase in impurities, there was a 20% increase in hardness [9]. According to the EDS analysis (Figure 3), zirconium and niobium are also present in this area, which forms an and is responsible for higher hardness than in the case of pure chromium [10].

The rest of indents extend into the matrix where zirconium is the dominant element. The hardness measured at the coating-matrix interface gradually decreased linearly with distance from ± 7 GPa to ± 6 GPa (Graph 4). At the same time, the concentration of chromium decreases in the direction from the oxide layer and coating to the material matrix. This corresponds with the measured hardness values since chromium forms intermetallic phases with both niobium and zirconium [11].

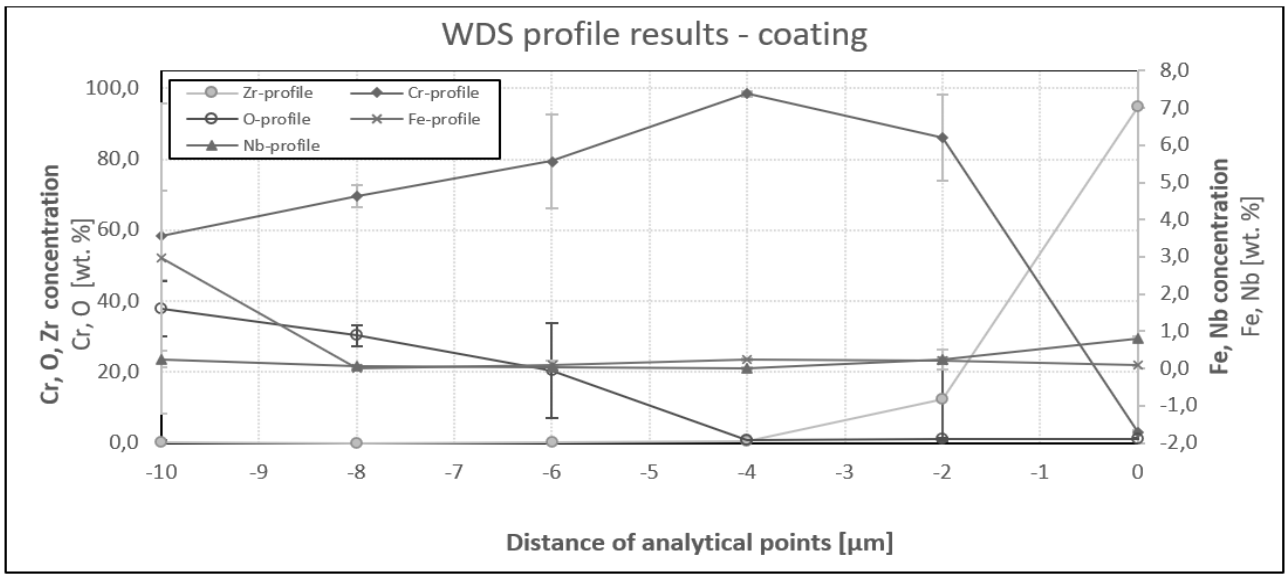

Graph 1 *Detailed composition of the oxidation layer and coating*

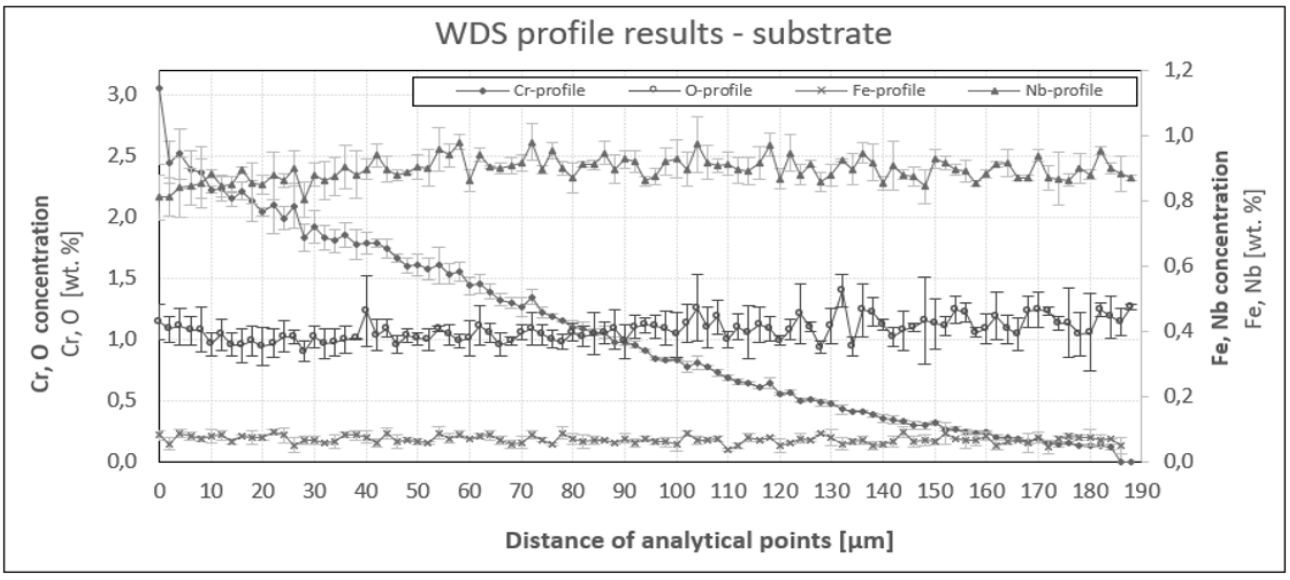

Graph 2 *Detailed composition of the Zr-matrix*

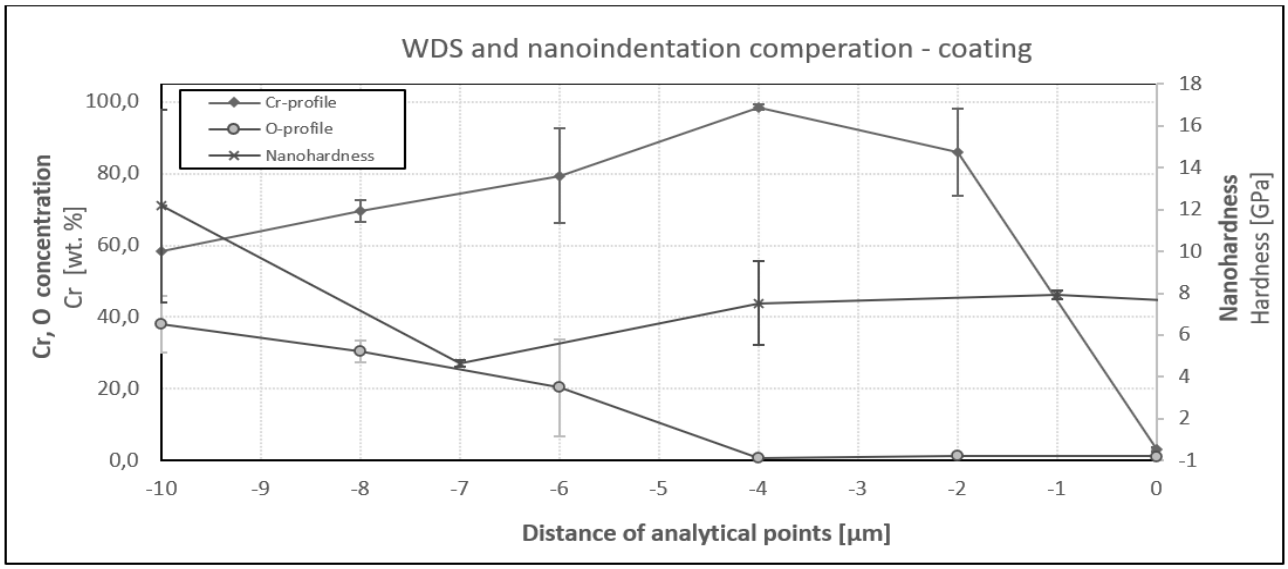

Graph 3 *Comparison of Cr, O-line profiles and nanohardness changein the area of oxidation layer and coating*

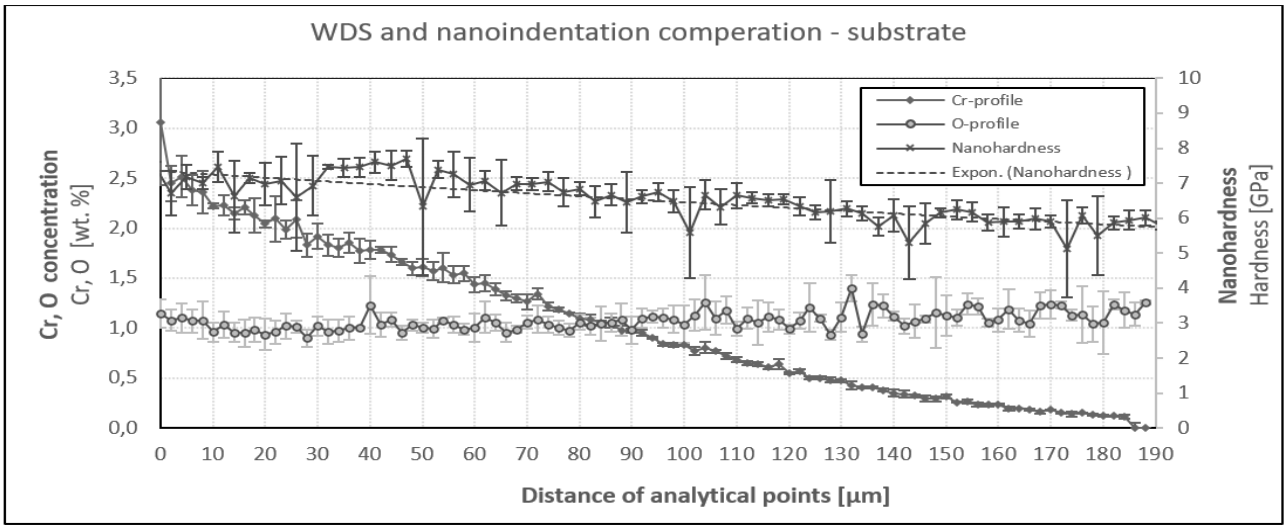

Graph 4 *Comparison of Cr, O-line profiles and nanohardness change in the area of Zr-matrix*

EDS analysis provided image support for the diffusion of Cr in the Zr-substrate (Figure 2). A detailed EDS map of the oxide layer, coating and part of the substrate showed diffusion of Cr into the substrate. It forms a visible layer of 1 µm width at a distance of 0 µm. According to WDS analysis, the chromium content here is 3.06 µm. And at the exact moment, Zr diffuses into the coating along grain boundaries. The same effect was described for Zircaloy-4 alloy in [1]. In this contribution, it is also confirmed that niobium diffuses into coating along the grain boundaries.

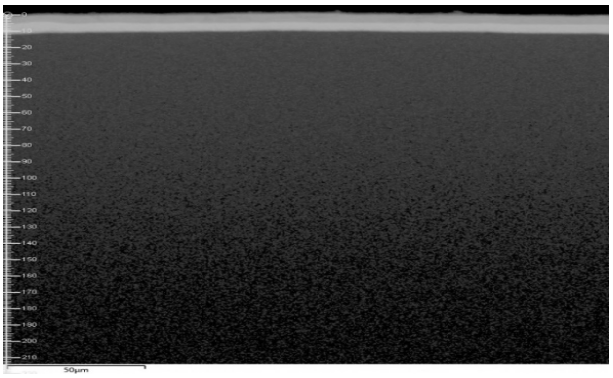

Fig. 2 *EDS Layered image of the Cr-content*

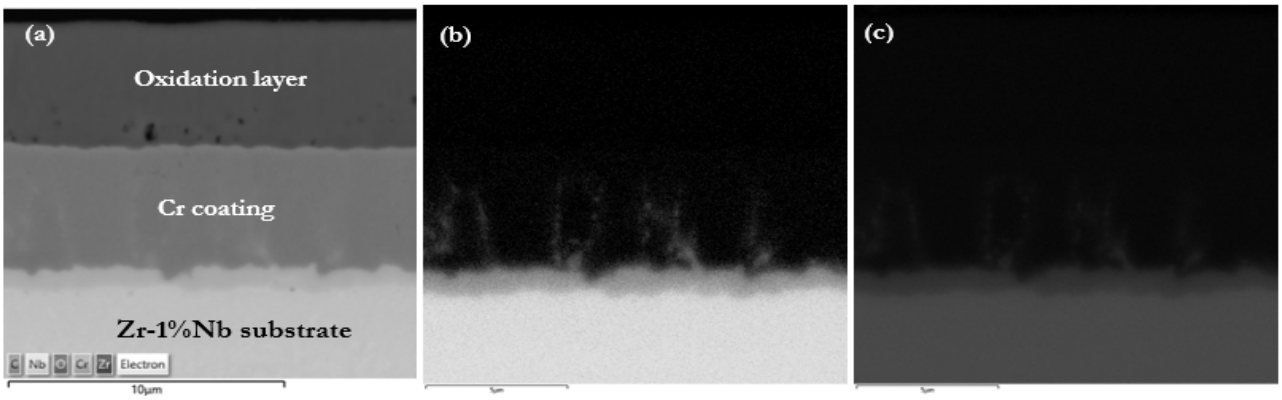

Fig. 3 *(a) EDS Layered image; (b) Nb La; (c) Zr La*

Tab. 1 *Wt. % of elements in the interference of oxidation layer, coating and substrate*

Distance (µm)	EDS map	Chemical concentration (wt. %)				
		Cr	Fe	Zr	Nb	O
-10		58.49	2.96	0.30	0.25	38.00
-8		69.58	0.01	0.01	0.08	30.32
-6		79.43	0.10	0.09	0.04	20.35
-4		98.44	0.24	0.55	0.01	0.76
-2		86.04	0.22	12.27	0.25	1.22
0		3.06	0.08	94.91	0.81	1.14
2		2.45	0.05	95.61	0.81	1.08

4 Conclusions

WDS analysis showed a Cr-diffusion into the Zr-matrix up to a distance of about 190 µm in the ATF fuel cladding exposed to the high temperature steam oxidation at 1200°C. The nanohardness of the material corresponds to the Cr concentration, i.e. decreases with decreasing Cr concentration.

The results were achieved using the methodology of automatic line-profile analysis to describe the change in chemical concentration and local mechanical properties developed for the ATF cladding measurements

Diffusion of zirconium and niobium into the Cr-oxidic phase along the grain boundaries was found out.

In the next step of this research, the sample will be subjected to TEM analysis to identify the Zr-Nb phase in the coating as well as the testing of the ATF cladding alloy under high temperature oxidation at higher temperatures at different time periods. Tested ATF materials within presented publication are the reference state for the neutron-irradiated ATFs to 0.3 dpa which will be investigated in the further study under the developed methodology based on the previos results obtained on neutron-irradiated structural materials [12].

Acknowledgement

This article was created with the support of the Technology Agency of The Czech Republic in the Theta program as the part of the project No. TK03020169.

References

[1] BRACHET J-CHRISTOPHE, ROUESNE E, RIBIS J, GUILBERT T, URVOY S, NONY G, TOFFOLON-MASCLET C, LE SAUX M, CHAABANE N, PALANCHER H, DAVID A, BISCHOFF J, AUGEREAU J, POUILLIER E, "High Temperature Steam Oxidation of Chromium-Coated Zirconium-Based Alloys: Kinetics and Process", *Corrosion Science* (2020), doi: https://doi.org/10.1016/j.corsci.2020.108537

[2] GÁVELOVÁ, P., HALODOVÁ, P., KŘIVSKÁ, B., CORREA, C. A., KREJČÍ, J., ŠEVEČEK, M., ROSNECKÝ, V.: Microstructure of Zirconium Fuel Claddings: TEM and EBSD Studies of As-Received and Neutron-Irradiated Materias, In: *Manufacturing Technology,* vol. 20, no. 6, p. 720-727

[3] GÁVELOVÁ, P., HALODOVÁ, P., LIBERA, O.; PROKŮPKOVÁ, I., VRTÍLKOVÁ, V.; KREJČÍ, J.: Experimental verification of phase diagram calculations of Zr-based alloys after high-temperature oxidation, In: *Defect and Diffusion Forum 2020*, vol. 405, p. 351 – 354

[4] MALERBA, L.; AL MAZOUZI, A.; BERTOLUS, M.; COLOGNA, M.; EFSING, P.; JIANU, A.; et al. Materials for Sustainable Nuclear Energy: A European Strategic Research and Innovation Agenda for All Reactor Generations. *MDPI* [Online] 2022. https://www.mdpi.com/1996-1073/15/5/1845/htm (accessed Sept 13, 2022)

[5] KESSEDJIAN, G.; JURADO, B.; AICHE, M.; BARREAU, G. PHYSICS LETTERS B, 692th ed. [online]; pp 297–301. https://www.sciencedirect.com/science/article/pii/S0370269310009007 (accessed Sept 13, 2022)

[6] KREJČÍ J., ŠEVEČEK M., CVRČEK L., KABÁTOVÁ J., MANOCH F.: Chromium and Chromium Nitride Coated Cladding for Nuclear Reactor Fuel, *Conference EUROCORR 2017*, Prague

[7] YANG, J.; STEGMAIER, U.; TANG, CH.; STEINBRUCK, M.; GROSSE, M.; WANG, S.; SEIFERT, H. High temperature Cr-Zr interaction of two types of Cr-coated Zr alloys in inert gas environment. *Journal of Nuclear Materials* [Online] 2021. https://www.sciencedirect.com/science/article/pii/S0022311521000295 (accessed Sept 13, 2022)

[8] ABU-SHGAIR, K.; et al. Characterizing crystalline chromium oxide thin film growth parameters. *Re-views on Advanced Materials Science* [Online] 2010. https://www.researchgate.net/publication/228416200_Characterizing_crystalline_chromium_oxide_thin_film_growth_parameters (accessed July 12, 2022)

[9] IN-CHUL, CH.; BRANDL, CH.; SCHWAIGER, R. Thermally activated dislocation plasticity in body-centered cubic chromium studied by high-temperature nanoindentation. *Materials Science and Engineering* [Online] 2022. https://www.sciencedirect.com/science/article/pii/S1359645417306808 (accessed Sept 12, 2022)

[10] KEWEI, L.; SHUANGMING, L. Microstructure characterization and mechanical properties of a Laves-phase alloy based on Cr2Nb. *International Journal of Refractory Metals and Hard Materials* [Online] 2013. https://www.researchgate.net/publication/271635980_Microstructure_characterization_and_mechanical_properties_of_a_Laves-phase_alloy_based_on_Cr2Nb (accessed Sept 12, 2022)

[11] OKAMOTO, H.; SCHLESINGER, M.; MUELLER, E. Cr (Chromium) Binary Alloy Phase Diagrams. *ASM Handbook*: Volume 3, Alloy phase diagrams, 3rd ed.; 2016

[12] BUBLÍKOVÁ, P., HALODOVÁ, P., , FOKT, M., NAMBURI, H. K., ROSNECKÝ, V., PROCHÁZKA, J., DUCHOŇ, J., VOJTĚCH, D.: Neutron irradiated reactor internals: An applied methodology for specimen preparation and Post Irradiation Examination by electron microscopy methods, In: *Manufacturing Technology,* vol. 18, no. 4, p. 545-551